Journal of proteome research

pubs.acs.org/jpr

Technical Note

Low Volume in Vitro Diagnostic Proton NMR Spectroscopy of Human Blood Plasma for Lipoprotein and Metabolite Analysis: Application to SARS-CoV-2 Biomarkers

Samantha Lodge, Philipp Nitschke, Ruey Leng Loo, Torben Kimhofer, Sze-How Bong, Toby Richards, Sofina Begum, Manfred Spraul, Hartmut Schaefer, John C. Lindon, Elaine Holmes,* and Jeremy K. Nicholson*

Cite This: *J. Proteome Res.* 2021, 20, 1415−1423

Read Online

ACCESS | Metrics & More | Article Recommendations | Supporting Information

ABSTRACT: The utility of low sample volume in vitro diagnostic (IVDr) proton nuclear magnetic resonance (^{1}H NMR) spectroscopic experiments on blood plasma for information recovery from limited availability or high value samples was exemplified using plasma from patients with SARS-CoV-2 infection and normal controls. ^{1}H NMR spectra were obtained using solvent-suppressed 1D, spin−echo (CPMG), and 2-dimensional J-resolved (JRES) spectroscopy using both 3 mm outer diameter SampleJet NMR tubes (100 μL plasma) and 5 mm SampleJet NMR tubes (300 μL plasma) under in vitro diagnostic conditions. We noted near identical diagnostic models in both standard and low volume IVDr lipoprotein analysis (measuring 112 lipoprotein parameters) with a comparison of the two tubes yielding R^2 values ranging between 0.82 and 0.99 for the 40 paired lipoprotein parameters samples. Lipoprotein measurements for the 3 mm tubes were achieved without time penalty over the 5 mm tubes as defined by biomarker recovery for SARS-CoV-2. Overall, biomarker pattern recovery for the lipoproteins was extremely similar, but there were some small positive offsets in the linear equations for several variables due to small shimming artifacts, but there was minimal degradation of the biological information. For the standard untargeted 1D, CPMG, and JRES NMR experiments on the same samples, the reduced signal-to-noise was more constraining and required greater scanning times to achieve similar differential diagnostic performance (15 min per sample per experiment for 3 mm 1D and CPMG, compared to 4 min for the 5 mm tubes). We conclude that the 3 mm IVDr method is fit-for-purpose for quantitative lipoprotein measurements, allowing the preparation of smaller volumes for high value or limited volume samples that is common in clinical studies. If there are no analytical time constraints, the lower volume experiments are equally informative for untargeted profiling.

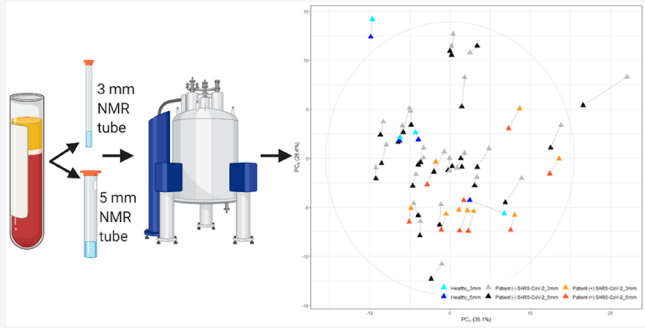

KEYWORDS: *blood plasma, ^{1}H NMR spectroscopy, IVDr, miniaturization, metabolic phenotyping, biomarkers, low volume, 3 mm NMR tubes, SARS-CoV-2, spin−echo, J-resolved*

INTRODUCTION

High field proton NMR spectroscopy of biofluids coupled with pattern recognition methods have been applied extensively to problems in metabolic biochemistry, toxicology, and experimental diagnostics for more than three decades.[1−4] More recently, data analytic procedures such as curve and regression fitting have been used to extract quantitative lipoprotein and metabolic data from 1-dimensional blood plasma and urine spectra.[5−7] The mainstay of most biofluid NMR studies is the standard 5 mm outer diameter liquid state NMR tubes (with 5 mm NMR probes) used in the vast majority of all high-resolution chemical and biochemical experiments. A range of tube sizes is also widely available, for example 1 mm to 10 mm for high resolution studies and 15 mm 25 mm tubes for wide-bore NMR applications. Each tube size has been optimized for a particular sample volume range and there are sensitivity consequences for using smaller sample volumes at the same sample concentration because the absolute analyte mass in the probe is reduced proportionately.

Of note, the signal-to-noise ratio (S/N) in an NMR experiment is proportional to the absolute analyte mass in the receiver coil; halving this will require a quadruple number of scans to obtain the same S/N in an identical probe with identical

Received: October 14, 2020
Published: January 23, 2021

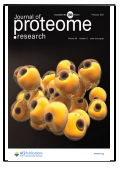

filling factor (the % of the receiver coil containing the analytes).[8] This can result in severe spectral acquisition time penalties for low volume samples or compromised S/N ratios with weaker diagnostic performance. It is rare to have volume limitations for urine samples even in small animal studies.[6] However, blood plasma or serum samples are commonly available in limited amounts, such as those on small animals or infants, where it would be unethical to withdraw large amounts of blood, or in situations where the samples that are available are needed for multiple parallel metabolic studies involving multiple technologies. The latter applies to systemic metabolic studies on COVID-19, where attempts to uncover the complex metabolic sequelae via multiple orthogonal technologies often applied on the same samples,[9] leading to analytical priority decisions that may reduce the number of analytical options per sample. ^{1}H NMR spectroscopy of biofluids for in vitro diagnostics in standard 5 mm tubes requires ca. 0.3 mL of sample.[10,11]

The standard IVDr NMR methods for blood plasma lipoprotein measurements utilize 5 mm tubes with a minimal sample requirement of 300 μL (plus 300 μL buffer) as determined by a validated IVDr protocol,[12] while mass spectrometry requires typically 10−30 μL per assay.[13−15] Any reduction in NMR preparative volumes will therefore provide more opportunities for complementary analytical coverage of the same sample using additional spectroscopic assays. Here the use of 100 μL plasma in 3 mm SampleJet tubes was investigated using a modified IVDr method and longer scanning times and compared with standard IVDr methods in 5 mm SampleJet tubes using a cohort of control, SARS-CoV-2 positive patients, and SARS-CoV-2 negative patients.

MATERIALS AND METHODS

Patient Enrolment and Sample Collection

Blood plasma and serum samples were collected from a cohort of adult individuals in a study initiated at Fiona Stanley Hospital by the Covid Research Response team (https://research-au.net/covid-research-response/) as part of the International Severe Acute Respiratory and Emerging Infection Consortium (ISARIC)/ World Health Organisation (WHO) pandemic trail framework (SMHS Research Governance Office PRN:3976 and Murdoch University Ethics no. 2020/052). Three groups of participants were recruited: (i) patients who presented with SARS-CoV-2 disease symptoms and subsequently tested positive for SARS-CoV-2 infection from upper and/or lower respiratory tract swabs by RT-PCR (n = 9 participants); (ii) blood samples from patients with SARS-CoV-2 disease symptoms and who had tested negative by RT-PCR (n = 27 participants); and (iii) healthy controls with no respiratory symptoms (n = 4 participants) who were enrolled as volunteers, according to Murdoch University Ethics no. 2020/053. The demographic data are shown in Table S1.

Sample Preparation for NMR Analysis

Plasma samples were centrifuged and processed according to a standard protocol.[10,11] Prior to NMR analysis, frozen plasma samples were thawed at 20 °C for 30 min and centrifuged for 10 min at 13 000g at 4 °C. Plasma samples were prepared using both 5 mm SampleJet NMR tubes, following the recommended procedures for in vitro analytical and diagnostics procedures,[12] and 3 mm SampleJet NMR tubes. For the standard sample preparation for 5 mm NMR tubes, each aliquot of 300 μL of plasma was mixed with 300 μL phosphate buffer (75 mM Na_2HPO_4, 2 mM NaN_3, 4.6 mM sodium trimethylsilyl propionate-[2,2,3,3−$^2H_4$] (TSP) in 80% D_2O, pH 7.4 ± 0.1),[11] mixed and spun for 5 s to ensure all liquid is at the bottom of the tube and transferred to a 5 mm SampleJet tube. For the sample preparation using 3 mm SampleJet NMR tubes, each aliquot of 100 μL of plasma was mixed with 100 μL phosphate buffer, mixed and spun for 5 s and 180 μL was transferred to a 3 mm tube for analyses. The 3 mm SampleJet NMR tubes require less than a third of the sample volume compared to the 5 mm SampleJet NMR tubes.

^{1}H NMR Spectroscopy Data Acquisition and Processing Parameters

NMR spectroscopic analyses were performed on a 600 MHz Bruker Avance III HD spectrometer equipped with a 5 mm BBI probe and fitted with the Bruker SampleJet robot cooling system set to 5 °C. A full quantitative calibration was completed prior to the analysis using a previously described protocol.[11] All experiments were completed using the Bruker in vitro diagnostics research (IVDr) methods.[16] For samples prepared in both 3 mm SampleJet and 5 mm SampleJet NMR tubes, three experiments were carried out in automation mode, amounting to a total of 12.5 min acquisition time per sample: standard 1D experiment with solvent presaturation with gradient (32 scans, 96K data points, spectral width of 30 ppm), a Carr−Purcell−Meiboom−Gill (CPMG) spin−echo experiment (32 scans, 72K data points, spectral width of 20 ppm) and a 2-dimensional J-resolved experiment (40 t_1 increments with 2 scans each). In addition, for the samples prepared in both 3 mm SampleJet NMR tubes, three further experiments were completed using higher scan option for each experiment amounting to a total acquisition time of 38 min per sample: standard 1D experiment with solvent presaturation (128 scans, 96K data points, spectral width of 30 ppm), a Carr−Purcell−Meiboom−Gill (CPMG) spin−echo experiment (128 scans, 72K data points, spectral width of 20 ppm) and a 2-dimensional J-resolved experiment (40 t_1 increments with 4 scans each). Data were processed in automation using Bruker Topspin 3.6.2 and ICON NMR to achieve phasing and baseline correction.[17]

A total of 112 lipoprotein parameters for each sample were generated using the Bruker IVDr Lipoprotein Subclass Analysis (B.I.-LISA) method by mathematically interrogating and quantifying the $-(CH_2)_n$ at δ = 1.25 and $-CH_3$ at δ = 0.80 peaks of the 1D spectrum after normalization to the Bruker QuantRef manager within Topspin using a PLS-2 regression model.[12] The lipoprotein data describe chemical components of cholesterol, free cholesterol, phospholipids, triglycerides, Apolipoproteins A1/A2/B100 and the B100/A1 ratio in different density classes: high-density lipoprotein (HDL, density 1.063−1.210 kg/L), intermediate-density lipoprotein (IDL, density 1.006−1.019 kg/L) low-density lipoprotein (LDL, density 1.09−1.63 kg/L), and very low-density lipoprotein (VLDL, 0.950−1.006 kg/L). The main lipoprotein classes HDL, LDL, VLDL were subdivided into different density subclasses (LDL-1:1.019−1.031 kg/L, LDL-2:1.031−1.034 kg/L, LDL-3:1.034−1.037 kg/L, LDL-4:1.037−1.040 kg/L, LDL-5:1.040−1.044 kg/L, LDL-6:1.044−1.063 kg/L), and the HDL subfractions into 4 different density classes (HDL-1 1.063−1.100 kg/L, HDL-2 1.100−1.125 kg/L, HDL-3 1.125−1.175 kg/L, and HDL-4 1.175−1.210 kg/L), the VLDL subfractions divided into 5 different density classes. A list of the 112 lipoprotein subfractions and parameter annotations is provided in Table S2.

https://dx.doi.org/10.1021/acs.jproteome.0c00815
J. Proteome Res. 2021, 20, 1415−1423

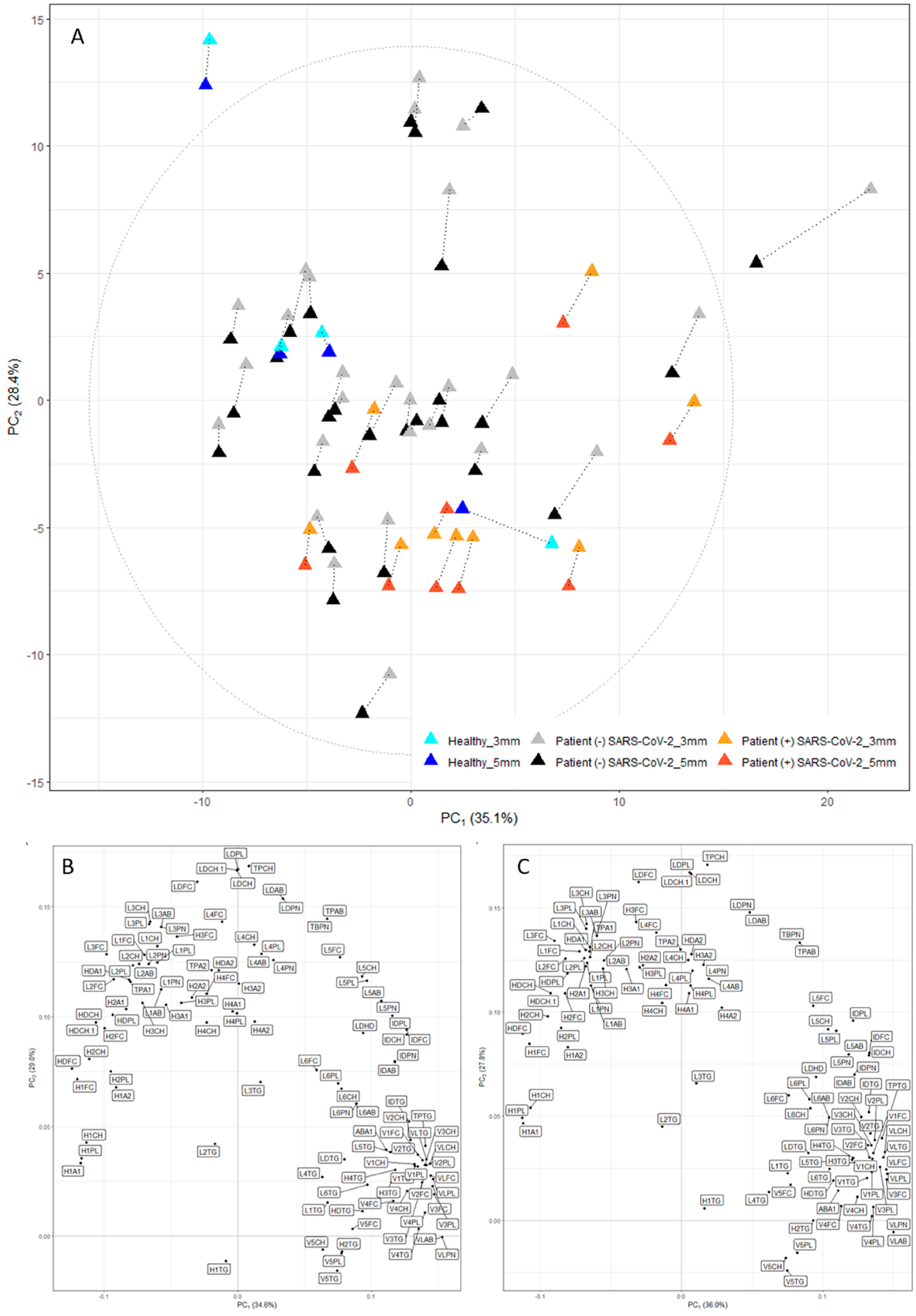

Figure 1. PCA of lipoprotein concentrations using 3 mm and 5 mm SampleJet NMR tubes: (A) PCA scores plot showing both 3 mm and 5 mm SampleJet NMR tubes were substantially similar. PCA loadings plots for the (B) 5 mm NMR SampleJet tubes only; and (C) 3 mm NMR SampleJet tubes only.

https://dx.doi.org/10.1021/acs.jproteome.0c00815
J. Proteome Res. 2021, 20, 1415−1423

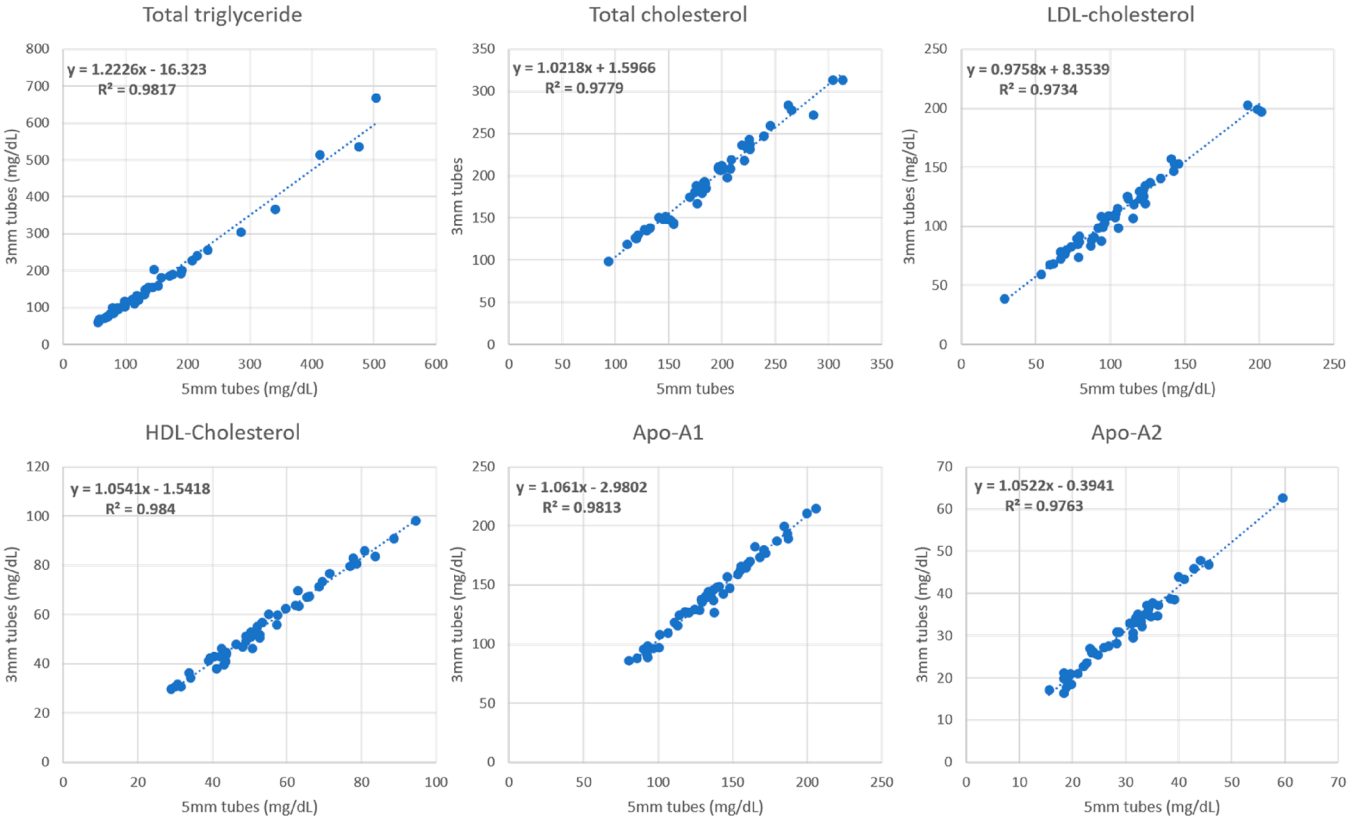

Figure 2. Comparison of lipoprotein concentrations for the six main fractions using 5 mm SampleJet NMR tubes and 3 mm SampleJet NMR tube by the Bruker quantitative IVDr method. Total triglyceride; total cholesterol; LDL-cholesterol; HDL-cholesterol; Apolipoprotein A1; and apolipoprotein A2. The fit equation and R^2 are shown for each lipoprotein parameter.

NMR Data Analysis

The 1D and CPMG NMR spectral data sets were referenced to glucose at δ = 5.25 using open source MetaboM8 software packages available from GitHub (github.com/tkimhofer/metabom8, version 0.1)[18] and corrected for baseline offset. Spectral regions corresponding to the residual water resonance signal (δ = 4.60−4.85) and those predominantly noise (δ < 0.25 and δ > 9.5) were excluded from analyses. The remaining spectral segments were normalized using a probabilistic quotient method,[19] mean-centered and scaled to unit-variance prior to multivariate modeling. Principal component analysis (PCA) was used to describe the underlying composition in quantitative lipoprotein, 1D and CMPG spectral data sets and to identify the clustering of healthy controls, SARS-CoV-2 positive, and SARS-CoV-2 negative individuals.

RESULTS AND DISCUSSION

Quantitative Comparison of 5 mm and 3 mm Lipoprotein Fractions

One of the real-world problems in studying complex emergent diseases such as SARS-CoV-2 is that patient sampling is often sparse or incomplete and multiple subsamples are needed to cover a large number of biochemical tests and different mass spectrometric assays. This problem is also applicable where there are limited sample volumes, including studies on children and babies. Here the use of reduced sample volumes was investigated using 3 mm SampleJet NMR tubes (100 μL of plasma required) compared against the standard 5 mm SampleJet tube method (300 μL) for blood plasma with the standard lipoprotein IVDr quantification employing three different study cohorts—SARS-CoV-2 positive, SARS-CoV-2 negative, and healthy control samples.

IVDr methods extracted 112 lipoprotein parameters from the 1D spectra of the same samples either in 3 mm or 5 mm tubes, both obtained using 32 scans (4 min experiment). The overall PCA mapping of a mixture of the different patient and sample tubes with the different volumes are shown in Figure 1 with identical biological samples connected by dotted lines. The overall statistical distribution of the samples was maintained, i.e., multivariate biological variation exceeded the analytical variation and that thus the outputs of the two analytical procedures were substantially equivalent. However, some minor discrepancies for some samples were observed due to differential field inhomogeneities (shimming artifacts) that slightly influence the quantitative output of the IVDr fitting algorithms for some parameters. The PCA loading plots for the samples prepared in 5 mm and 3 mm SampleJet NMR tubes are nearly identical (Figures 1B and 1C), indicating equivalent biomarker information recovery. A detailed biological description of the meaning of these parameters in relation to the complex biochemical of SARS-CoV-2 positivity is reported elsewhere.[9] OPLS-DA was applied to the 5 mm and 3 mm lipoprotein data sets to compare the healthy controls and the SARS-CoV-2 positive patients. The different size tubes both yielded an AUROC of 1.0 with the coefficient plots yielding the same lipoprotein parameters driving the SARS-CoV-2 signature (Figure S1).

The quantitative relationships between the different sample volumes is illustrated in Figure 2 for the main six lipoprotein fractions. In all cases, there was a high degree of linearity with exceptionally high coefficients of determination (R^2 in the range

https://dx.doi.org/10.1021/acs.jproteome.0c00815
J. Proteome Res. 2021, 20, 1415−1423

Table 1. Quantitative Comparison of 5 mm and 3 mm Lipoprotein Fractions, Showing the Fit Equation and R^2 for Each Fraction between Identical Paired Samples in 5 mm versus 3 mm NMR Tubes (n = 40)

lipoprotein fraction	fit equation	R^2	lipoprotein fraction	fit equation	R^2
Triglyceride	$y = 1.23x - 16.32$	0.98	Phospholipids VLDL-3	$y = 1.15x - 0.31$	0.98
Cholesterol	$y = 1.02x + 1.60$	0.98	Phospholipids VLDL-4	$y = 1.12x - 0.43$	0.98
LDL-Cholesterol	$y = 0.98x + 8.35$	0.97	Phospholipids VLDL-5	$y = 1.09x - 0.18$	0.94
HDL-Cholesterol	$y = 1.05x - 1.54$	0.98	Triglycerides LDL-1	$y = 1.09x - 0.71$	0.91
Apo-A1	$y = 1.06x - 2.98$	0.98	Triglycerides LDL-2	$y = 0.95x + 0.16$	0.93
Apo-A2	$y = 1.05x - 0.39$	0.98	Triglycerides LDL-3	$y = 0.99x + 0.01$	0.99
Apo-B100	$y = 1.00x + 5.15$	0.95	Triglycerides LDL-4	$y = 0.99x + 0.15$	0.94
LDL-Chol/HDL-Chol	$y = 1.00x + 0.09$	0.98	Triglycerides LDL-5	$y = 1.02x + 0.21$	0.90
Apo-B100/Apo-A1	$y = 1.00x + 0.01$	0.98	Triglycerides LDL-6	$y = 1.12x - 0.28$	0.96
Total particle number	$y = 1.00x + 93.52$	0.95	Cholesterol LDL-1	$y = 1.08x - 3.62$	0.94
VLDL particle number	$y = 1.11x - 13.84$	0.99	Cholesterol LDL-2	$y = 1.02x + 0.17$	0.94
IDL particle number	$y = 1.04x + 6.38$	0.92	Cholesterol LDL-3	$y = 1.01x + 0.52$	0.95
LDL particle number	$y = 0.97x + 106.17$	0.96	Cholesterol LDL-4	$y = 0.95x + 2.02$	0.96
LDL-1 particle number	$y = 1.07x - 29.44$	0.93	Cholesterol LDL-5	$y = 0.97x + 3.09$	0.87
LDL-2 particle number	$y = 1.02x + 3.27$	0.92	Cholesterol LDL-6	$y = 1.10x - 0.12$	0.93
LDL-3 particle number	$y = 1.03x + 3.01$	0.95	Free cholesterol LDL-1	$y = 1.09x - 0.79$	0.95
LDL-4 particle number	$y = 0.94x + 26.57$	0.96	Free cholesterol LDL-2	$y = 0.99x + 0.42$	0.92
LDL-5 particle number	$y = 0.97x + 40.30$	0.85	Free cholesterol LDL-3	$y = 1.02x + 0.26$	0.94
LDL-6 particle number	$y = 1.16x - 22.01$	0.93	Free cholesterol LDL-4	$y = 0.96x + 0.75$	0.93
Triglycerides VLDL	$y = 1.74x - 2.93$	0.98	Free cholesterol LDL-5	$y = 0.95x + 1.11$	0.82
Triglycerides IDL	$y = 1.22x - 0.87$	0.99	Free cholesterol LDL-6	$y = 1.15x + 0.22$	0.88
Triglycerides LDL	$y = 1.03x + 0.82$	0.91	Phospholipids LDL-1	$y = 1.09x - 2.22$	0.93
Triglycerides HDL	$y = 1.14x - 0.55$	0.93	Phospholipids LDL-2	$y = 1.02x - 0.10$	0.94
Cholesterol VLDL	$y = 1.13x - 2.86$	0.99	Phospholipids LDL-3	$y = 1.03x + 0.08$	0.94
Cholesterol IDL	$y = 1.14x - 0.19$	0.95	Phospholipids LDL-4	$y = 0.95x + 1.05$	0.96
Cholesterol LDL	$y = 0.98x + 8.54$	0.97	Phospholipids LDL-5	$y = 0.95x + 1.81$	0.87
Cholesterol HDL	$y = 1.05x - 1.54$	0.98	Phospholipids LDL-6	$y = 1.12x - 0.44$	0.92
Free cholesterol VLDL	$y = 1.09x - 0.51$	0.99	Apo-B LDL-1	$y = 1.07x - 1.62$	0.93
Free cholesterol IDL	$y = 1.17x - 0.20$	0.95	Apo-B LDL-2	$y = 1.02x + 0.18$	0.92
Free cholesterol LDL	$y = 1.00x + 2.28$	0.96	Apo-B LDL-3	$y = 1.03x + 0.16$	0.95
Free cholesterol HDL	$y = 1.09x + 0.29$	0.96	Apo-B LDL-4	$y = 0.94x + 1.46$	0.96
VLDL phospholipids	$y = 1.07x - 0.10$	0.99	Apo-B LDL-5	$y = 0.97x + 2.21$	0.85
IDL phospholipids	$y = 1.16x - 0.32$	0.98	Apo-B LDL-6	$y = 1.57x - 1.21$	0.93
LDL phospholipids	$y = 0.98x + 3.31$	0.97	Triglycerides HDL-1	$y = 0.95x + 0.68$	0.85
HDL phospholipids	$y = 1.07x - 3.50$	0.99	Triglycerides HDL-2	$y = 1.03x + 0.23$	0.89
Apo-A1 HDL	$y = 1.06x - 3.32$	0.97	Triglycerides HDL-3	$y = 1.14x - 0.09$	0.92
Apo-A2 HDL	$y = 1.05x - 0.50$	0.97	Triglycerides HDL-4	$y = 1.09x - 0.22$	0.99
Apo-B VLDL	$y = 1.11x - 0.76$	0.99	Cholesterol HDL-1	$y = 1.05x + 0.45$	0.98
Apo-B IDL	$y = 1.04x + 0.35$	0.92	Cholesterol HDL-2	$y = 1.00x + 0.71$	0.96
Apo-B LDL	$y = 0.97x + 5.39$	0.96	Cholesterol HDL-3	$y = 1.04x + 0.04$	0.98
Triglycerides VLDL-1	$y = 1.18x + 1.71$	0.95	Cholesterol HDL-4	$y = 0.96x - 0.19$	0.95
Triglycerides VLDL-2	$y = 1.15x - 0.67$	0.99	Free cholesterol HDL-1	$y = 1.08x + 0.44$	0.97
Triglycerides VLDL-3	$y = 1.20x - 1.58$	0.98	Free cholesterol HDL-2	$y = 1.07x + 0.20$	0.96
Triglycerides VLDL-4	$y = 1.13x - 0.51$	0.98	Free cholesterol HDL-3	$y = 1.09x + 0.18$	0.96
Triglycerides VLDL-5	$y = 1.04x - 0.04$	0.95	Free cholesterol HDL-4	$y = 1.03x + 0.20$	0.92
Cholesterol VLDL-1	$y = 1.16x - 0.59$	0.97	Phospholipids HDL-1	$y = 1.05x + 0.30$	0.98
Cholesterol VLDL-2	$y = 1.15x - 0.57$	0.99	Phospholipids HDL-2	$y = 1.00x + 1.01$	0.96
Cholesterol VLDL-3	$y = 1.16x - 0.44$	0.97	Phospholipids HDL-3	$y = 1.06x + 0.31$	0.98
Cholesterol VLDL-4	$y = 1.01x + 0.01$	0.96	Phospholipids HDL-4	$y = 0.98x - 0.53$	0.97
Cholesterol VLDL-5	$y = 1.09x - 0.30$	0.92	Apo-A1 HDL-1	$y = 1.05x + 0.30$	0.98
Free cholesterol VLDL-1	$y = 1.14x - 0.04$	0.97	Apo-A1 HDL-2	$y = 1.04x - 0.09$	0.98
Free cholesterol VLDL-2	$y = 1.18x - 0.30$	0.98	Apo-A1 HDL-3	$y = 1.05x - 0.11$	0.98
Free cholesterol VLDL-3	$y = 1.18x - 0.17$	0.99	Apo-A1 HDL-4	$y = 0.96x + 0.98$	0.96
Free cholesterol VLDL-4	$y = 1.05x + 0.04$	0.97	Apo-A2 HDL-1	$y = 1.06x + 0.12$	0.98
Free cholesterol VLDL-5	$y = 0.93x - 0.71$	0.92	Apo-A2 HDL-2	$y = 1.02x + 0.30$	0.95
Phospholipids VLDL-1	$y = 1.16x + 0.01$	0.96	Apo-A2 HDL-3	$y = 1.06x + 0.19$	0.96
Phospholipids VLDL-2	$y = 1.12x - 0.24$	0.99	Apo-A2 HDL-4	$y = 0.99x - 0.19$	0.97

https://dx.doi.org/10.1021/acs.jproteome.0c00815
J. Proteome Res. 2021, 20, 1415−1423

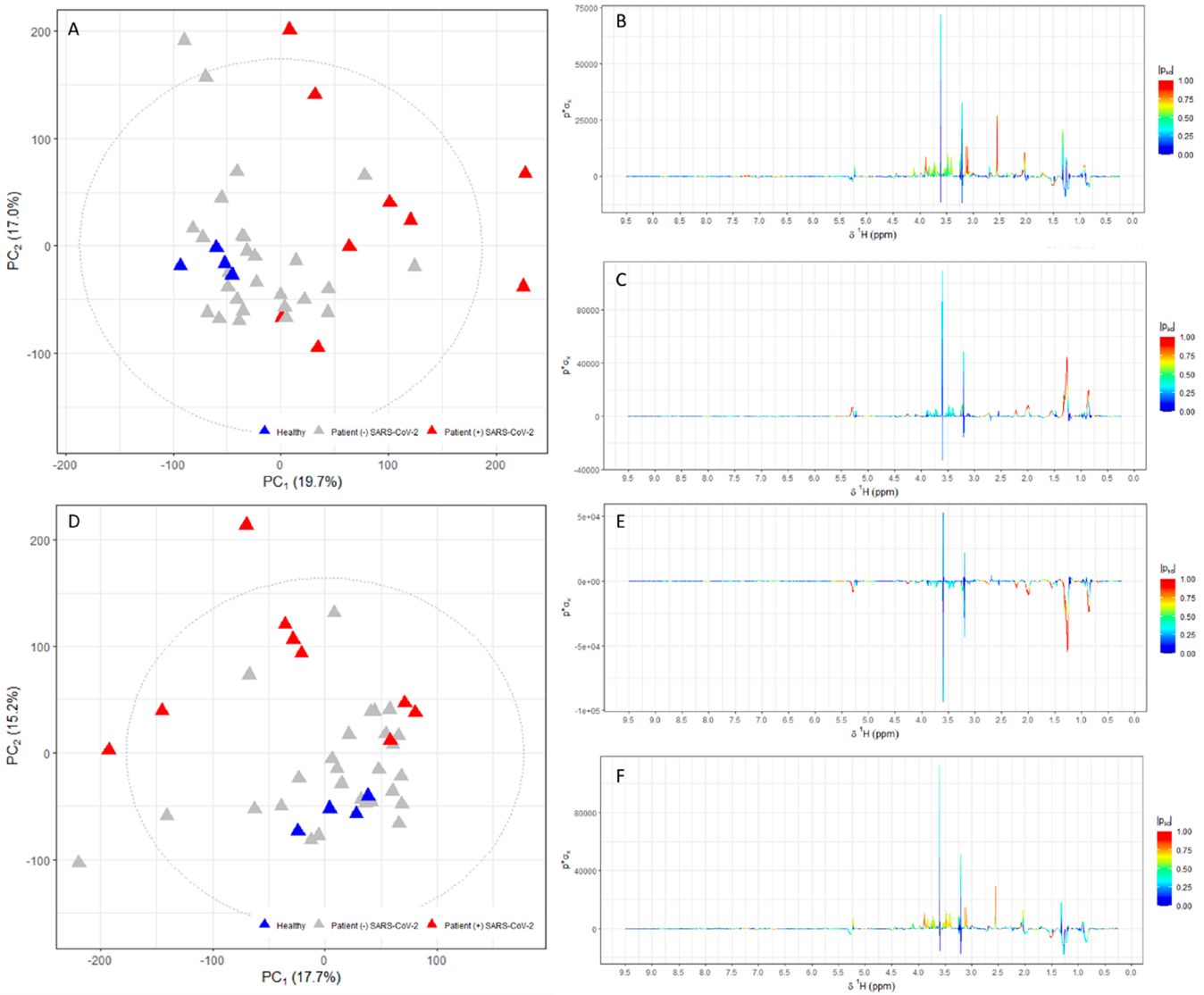

Figure 3. PCA scores and loading plots of the 1D spectral data for 5 mm and 3 mm SampleJet NMR analyses on 32 and 128 scans, respectively. (A) The PCA model for healthy controls, SARS-CoV-2 positive, and SARS-CoV-2 negative samples 1D spectra using 5 mm SampleJet NMR tubes with 32 scans. The ellipse indicates the boundary of the Hotelling's T2 statistic ($\alpha = 0.95$), which can be interpreted as a multivariate confidence interval; (B) the corresponding loadings plot for principal component 1 (PC1); and (C) principal component 2 (PC2). (D) The PCA model for healthy control, SARS-CoV-2 positive, and SARS-CoV-2 negative samples 1D spectra in 3 mm SampleJet NMR tubes using 128 scans; (E) the corresponding loadings for PC1; and (F) PC2.

0.82 to 0.99). However, there were some small positive offsets in the linear equations for several metabolites in certain compartments, e.g., LDL cholesterol and total triglycerides, although these need to be considered in relation to the overall magnitude of the lipoprotein concentration (Figure 2).

Individual linear equations for all 112 lipoproteins are listed in Table 1, with all but seven lipoprotein parameters (cholesterol LDL-5, free cholesterol LDL-6, free cholesterol LDL-5, phospholipids LDL-5, Apo-B LDL-5, triglycerides HDL-1, and triglycerides HDL-2) showing R^2 values of <0.9, indicating the 3 mm tubes can be used with confidence for all the measured IVDr lipoprotein parameters. The R^2 values and the calculated linear equations relating the variables for 3 mm and 5 mm tubes are shown in Table 1.

1D, CPMG, and JRES Spectral Data

Examination of the 1D and CPMG spectral data sets indicated that the signal-to-noise ratio of the 3 mm SampleJet NMR tubes was 2.8 times lower than that of the 5 mm, when 32 scans were used, which is due to the filling-effect of the 3 mm tubes in the 5 mm NMR probe volume. In particular, the metabolite signals at the aromatic regions were largely not detectable for the 3 mm NMR tubes with 32 scans (Figure S2). However, we expect that improved performance with a dedicated 3 mm NMR probe will be achievable. It was found that at least 128 scans for the 3 mm SampleJet NMR tubes was required in order for the aromatic peaks and some of the lower concentration metabolites to have sufficient signal-to-noise to be comparable to the standard 5 mm IVDr 32 scan method. For the JRES spectral data sets at least 4 scans are required in order to gain sufficient peak information (Figure S3).

PCA models were constructed for the 1D and CPMG spectral data sets separately, using healthy controls, SARS-CoV-2 negative, and the SARS-Cov-2 positive patients. Both the standard 32 scans (5 mm NMR tubes) and 128 scans (3 mm NMR tubes) showed highly comparable results for the 1D

https://dx.doi.org/10.1021/acs.jproteome.0c00815
J. Proteome Res. 2021, 20, 1415−1423

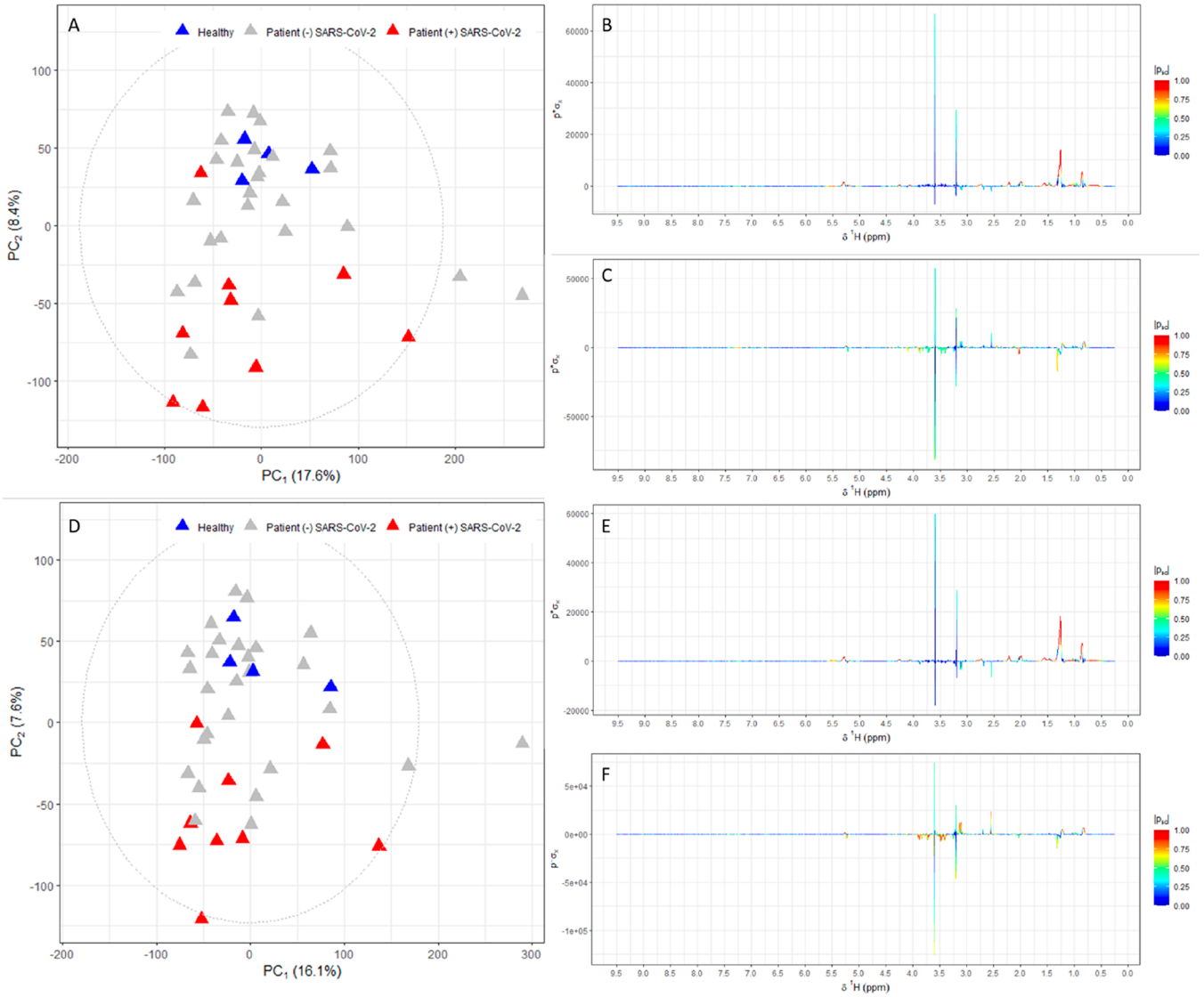

Figure 4. PCA scores and loading plots of the CPMG spectral data for 5 mm and 3 mm SampleJet NMR analyses on 32 and 128 scans, respectively. (A) The PCA model for healthy controls, SARS-CoV-2 positive, and SARS-CoV-2 negative samples CPMG spectra in 5 mm SampleJet NMR tubes using 32 scans. The ellipse indicates the boundary of the Hotelling's T2 statistic ($\alpha = 0.95$), which can be interpreted as a multivariate confidence interval; (B) the corresponding loadings plot for PC1; and (C) PC2. (D) The PCA model for healthy controls, SARS-CoV-2 positive, and SARS-CoV-2 negative samples CPMG spectra in 3 mm SampleJet NMR tubes using 128 scans; (E) the corresponding loadings for PC1; and (F) PC2.

(Figure 3) and CPMG (Figure 4) spectral data sets, but this was achieved at the cost of an approximately 4-fold increase in the total experimental time for each sample in the 3 mm NMR tubes.

When the PCA model was constructed for the CPMG spectral data set using 32 scans in the 3 mm NMR tubes, it was found that the PCA scores plot show clustering patterns that were similar to those seen in both the 5 mm tubes (32 scans) and the 3 mm (128 scans) SampleJet NMR tubes (Figure S4A). However, the loading plots clearly show that the clustering was dominated by the aliphatic molecules in the 3 mm NMR tubes with 32 scans (Figures S4B and S4C). The difference from the aromatic regions among the SARS-CoV-2 positive patients compared to the healthy and SARS-CoV-2 negative patients were not recovered using the 3 mm NMR tube with 32 scans when compared to the 5 mm NMR tubes using 32 scans (Figure S4D and S4E). This finding confirms that higher scan numbers are required for the 3 mm SampleJet NMR tubes in order to get the same level of metabolite signals information recovery from the healthy controls, SARS-CoV-2 positive and SARS-CoV-2 negative patients.

We conclude that all NMR experiments applied in this test series give substantially equivalent, differential diagnostic information for SARS-CoV-19 positive patient samples. The IVDr lipoprotein analysis is highly efficient and results in excellent quantitative agreement between the different sample volumes with no time penalty. However, the untargeted analysis is more sensitive to the reduced S/N in the smaller volume NMR tubes and therefore requires greater spectral accumulation time to recover similar metabolic biomarkers. We recommend that for clinical studies involving small numbers of samples and with limited sample volume, it would be feasible to adopt untargeted analysis using 3 mm NMR tubes with a higher scan number.

https://dx.doi.org/10.1021/acs.jproteome.0c00815
J. Proteome Res. 2021, 20, 1415−1423

■ ASSOCIATED CONTENT

Supporting Information

The Supporting Information is available free of charge at https://pubs.acs.org/doi/10.1021/acs.jproteome.0c00815.

Table S1: Full cohort demographic data; Table S2: Annotation of the keys used by the Bruker IVDr Lipoprotein Subclass Analysis (B.I.-LISA) method; Figure S1: OPLS-DA of the lipoprotein data set in the 5 mm (ns = 32) and 3 mm (ns = 32) SampleJet NMR tubes to compare healthy controls vs the SARS-CoV-2 positive patients; Figure S2: Overlay of a CPMG spectra of a SARS-CoV-2 positive patient analyzed in 5 mm SampleJet NMR tubes with 32 scans, and 3 mm NMR tube with 32 scans; Figure S3: JRES spectral overlays of (A) 5 mm SampleJet NMR tube with 2 scans (blue) and SampleJet 3 mm NMR tube with 2 scans; (B) 5 mm SampleJet NMR tube with 2 scans (blue) and 3 mm SampleJet NMR tube with 4 scans; Figure S4: PCA scores and loading plots of CPMG spectral data for 3 mm SampleJet NMR analyses using 32 scans and spectral overlays with principal component 2 loadings plots (PDF)

■ AUTHOR INFORMATION

Corresponding Authors

Elaine Holmes − *Australian National Phenome Centre, Health Futures Institute and Centre for Computational and Systems Medicine, Health Futures Institute, Murdoch University, Perth, WA 6150, Australia; Division of Systems Medicine, Department of Metabolism, Nutrition and Reproduction, Sir Alexander Fleming Building, Imperial College London, London SW7 2AZ, U.K.;* orcid.org/0000-0002-0556-8389; Email: elaine.holmes@murdoch.edu.au, elaine.holmes@imperial.ac.uk

Jeremy K. Nicholson − *Australian National Phenome Centre, Health Futures Institute and Centre for Computational and Systems Medicine, Health Futures Institute, Murdoch University, Perth, WA 6150, Australia; Institute of Global Health Innovation, Imperial College London, London SW7 2NA, U.K.*; Email: jeremy.nicholson@murdoch.edu.au, j.nicholson@imperial.ac.uk

Authors

Samantha Lodge − *Australian National Phenome Centre, Health Futures Institute, Murdoch University, Perth, WA 6150, Australia;* orcid.org/0000-0001-9193-0462

Philipp Nitschke − *Australian National Phenome Centre, Health Futures Institute, Murdoch University, Perth, WA 6150, Australia*

Ruey Leng Loo − *Australian National Phenome Centre, Health Futures Institute and Centre for Computational and Systems Medicine, Health Futures Institute, Murdoch University, Perth, WA 6150, Australia;* orcid.org/0000-0001-5307-5709

Torben Kimhofer − *Australian National Phenome Centre, Health Futures Institute and Centre for Computational and Systems Medicine, Health Futures Institute, Murdoch University, Perth, WA 6150, Australia;* orcid.org/0000-0001-7158-9930

Sze-How Bong − *Australian National Phenome Centre, Health Futures Institute, Murdoch University, Perth, WA 6150, Australia*

Toby Richards − *Division of Surgery, Medical School, Faculty of Health and Medical Sciences, University of Western Australia, Perth, WA 6150, Australia*

Sofina Begum − *Australian National Phenome Centre, Health Futures Institute, Murdoch University, Perth, WA 6150, Australia; Division of Systems Medicine, Department of Metabolism, Nutrition and Reproduction, Sir Alexander Fleming Building, Imperial College London, London SW7 2AZ, U.K.*

Manfred Spraul − *Bruker BIoSpin GmbH, Ettlingen 76275, Germany*

Hartmut Schaefer − *Bruker BIoSpin GmbH, Ettlingen 76275, Germany*

John C. Lindon − *Division of Systems Medicine, Department of Metabolism, Nutrition and Reproduction, Sir Alexander Fleming Building, Imperial College London, London SW7 2AZ, U.K.;* orcid.org/0000-0002-0916-6360

Complete contact information is available at: https://pubs.acs.org/10.1021/acs.jproteome.0c00815

Notes

The authors declare no competing financial interest.

■ ACKNOWLEDGMENTS

We thank The Spinnaker Health Foundation, WA, The McCusker Foundation, WA, The Western Australian State Government, and the MRFF for funding the Australian National Phenome Centre for this and related work. We thank the UK MRC for funding (SB), and the Department of Jobs, Tourism, Science and Innovation, Government of Western Australian Premier's Fellowship for funding RLL and EH; and ARC Laureate Fellowship funding for EH. We also would like to acknowledge the Western Australian Covid Research Response team (https://research-au.net/covid-research-response/), Dale Edgar, Edward Raby, Giuliana D'Aulerio, Kelly Beer, Rolee Kumar, Doug Robb, Joseph Miocevich, Dominic Mallonic, Michael Epis, Merrilee Needham, Daniel Fatovich, Aron Chakera, Thomas Gilbert, Nathanael Foo, @STRIVE WA, Candice Peel, Sheeraz Mohd, and Ali Alishum for the coordination, sampling, and biobanking of patient samples and clinical metadata.

■ REFERENCES

(1) Nicholson, J. K.; Buckingham, M. J.; Sadler, P. J. High resolution ^{1}H NMR studies of vertebrate blood and plasma. *Biochem. J.* **1983**, *211* (3), 605−15.

(2) Beckonert, O.; Keun, H. C.; Ebbels, T. M.; Bundy, J.; Holmes, E.; Lindon, J. C.; Nicholson, J. K. Metabolic profiling, metabolomic and metabonomic procedures for NMR spectroscopy of urine, plasma, serum and tissue extracts. *Nat. Protoc.* **2007**, *2* (11), 2692−703.

(3) Nicholson, J. K.; Wilson, I. D. High resolution proton magnetic resonance spectroscopy of biological fluids. *Prog. Nucl. Magn. Reson. Spectrosc.* **1989**, *21* (4−5), 449−501.

(4) Bales, J. R.; Nicholson, J. K.; Sadler, P. J. Two-dimensional proton nuclear magnetic resonance "maps" of acetaminophen metabolites in human urine. *Clin. Chem.* **1985**, *31* (5), 757−62.

(5) Gibson, R.; Lau, C. E.; Loo, R. L.; Ebbels, T. M. D.; Chekmeneva, E.; Dyer, A. R.; Miura, K.; Ueshima, H.; Zhao, L.; Daviglus, M. L.; Stamler, J.; Van Horn, L.; Elliott, P.; Holmes, E.; Chan, Q. The association of fish consumption and its urinary metabolites with cardiovascular risk factors: the International Study of Macro-/Micronutrients and Blood Pressure (INTERMAP). *Am. J. Clin. Nutr.* **2020**, *111* (2), 280−290.

(6) Lindon, J. C.; Keun, H. C.; Ebbels, T. M.; Pearce, J. M.; Holmes, E.; Nicholson, J. K. The Consortium for Metabonomic Toxicology (COMET): aims, activities and achievements. *Pharmacogenomics* **2005**, *6* (7), 691−9.
(7) Tzoulaki, I.; Castagne, R.; Boulange, C. L.; Karaman, I.; Chekmeneva, E.; Evangelou, E.; Ebbels, T. M. D.; Kaluarachchi, M. R.; Chadeau-Hyam, M.; Mosen, D.; Dehghan, A.; Moayyeri, A.; Ferreira, D. L. S.; Guo, X.; Rotter, J. I.; Taylor, K. D.; Kavousi, M.; de Vries, P. S.; Lehne, B.; Loh, M.; Hofman, A.; Nicholson, J. K.; Chambers, J.; Gieger, C.; Holmes, E.; Tracy, R.; Kooner, J.; Greenland, P.; Franco, O. H.; Herrington, D.; Lindon, J. C.; Elliott, P. Serum metabolic signatures of coronary and carotid atherosclerosis and subsequent cardiovascular disease. *Eur. Heart J.* **2019**, *40* (34), 2883−2896.
(8) Olson, D. L.; Norcross, J. A.; O'Neil-Johnson, M.; Molitor, P. F.; Detlefsen, D. J.; Wilson, A. G.; Peck, T. L. Microflow NMR: concepts and capabilities. *Anal. Chem.* **2004**, *76* (10), 2966−74.
(9) Kimhofer, T.; Lodge, S.; Whiley, L.; Gray, N.; Loo, R. L.; Lawler, N. G.; Nitschke, P.; Bong, S. H.; Morrison, D. L.; Begum, S.; Richards, T.; Yeap, B. B.; Smith, C.; Smith, K. C. G.; Holmes, E.; Nicholson, J. K. Integrative Modelling of Quantitative Plasma Lipoprotein, Metabolic and Amino Acid Data Reveals a Multi-organ Pathological Signature of SARS-CoV-2 Infection. *J. Proteome Res.* **2020**, *19* (11), 4442−4454.
(10) Loo, R. L.; Lodge, S.; Kimhofer, T.; Bong, S. H.; Begum, S.; Whiley, L.; Gray, N.; Lindon, J. C.; Nitschke, P.; Lawler, N. G.; Schafer, H.; Spraul, M.; Richards, T.; Nicholson, J. K.; Holmes, E. Quantitative In-Vitro Diagnostic NMR Spectroscopy for Lipoprotein and Metabolite Measurements in Plasma and Serum: Recommendations for Analytical Artefact Minimization with Special Reference to COVID-19/SARS-CoV-2 Samples. *J. Proteome Res.* **2020**, *19* (11), 4428−4441.
(11) Dona, A. C.; Jimenez, B.; Schafer, H.; Humpfer, E.; Spraul, M.; Lewis, M. R.; Pearce, J. T.; Holmes, E.; Lindon, J. C.; Nicholson, J. K. Precision high-throughput proton NMR spectroscopy of human urine, serum, and plasma for large-scale metabolic phenotyping. *Anal. Chem.* **2014**, *86* (19), 9887−94.
(12) Jimenez, B.; Holmes, E.; Heude, C.; Tolson, R. F.; Harvey, N.; Lodge, S. L.; Chetwynd, A. J.; Cannet, C.; Fang, F.; Pearce, J. T. M.; Lewis, M. R.; Viant, M. R.; Lindon, J. C.; Spraul, M.; Schafer, H.; Nicholson, J. K. Quantitative Lipoprotein Subclass and Low Molecular Weight Metabolite Analysis in Human Serum and Plasma by (1)H NMR Spectroscopy in a Multilaboratory Trial. *Anal. Chem.* **2018**, *90* (20), 11962−11971.
(13) Gray, N.; Zia, R.; King, A.; Patel, V. C.; Wendon, J.; McPhail, M. J.; Coen, M.; Plumb, R. S.; Wilson, I. D.; Nicholson, J. K. High-Speed Quantitative UPLC-MS Analysis of Multiple Amines in Human Plasma and Serum via Precolumn Derivatization with 6-Aminoquinolyl-N-hydroxysuccinimidyl Carbamate: Application to Acetaminophen-Induced Liver Failure. *Anal. Chem.* **2017**, *89* (4), 2478−2487.
(14) Whiley, L.; Nye, L. C.; Grant, I.; Andreas, N.; Chappell, K. E.; Sarafian, M. H.; Misra, R.; Plumb, R. S.; Lewis, M. R.; Nicholson, J. K.; Holmes, E.; Swann, J. R.; Wilson, I. D. Ultrahigh-Performance Liquid Chromatography Tandem Mass Spectrometry with Electrospray Ionization Quantification of Tryptophan Metabolites and Markers of Gut Health in Serum and Plasma-Application to Clinical and Epidemiology Cohorts. *Anal. Chem.* **2019**, *91* (8), 5207−5216.
(15) Huynh, K.; Barlow, C. K.; Jayawardana, K. S.; Weir, J. M.; Mellett, N. A.; Cinel, M.; Magliano, D. J.; Shaw, J. E.; Drew, B. G.; Meikle, P. J. High-Throughput Plasma Lipidomics: Detailed Mapping of the Associations with Cardiometabolic Risk Factors. *Cell Chem. Biol.* **2019**, *26* (1), 71−84.
(16) Monsonis Centelles, S.; Hoefsloot, H. C. J.; Khakimov, B.; Ebrahimi, P.; Lind, M. V.; Kristensen, M.; de Roo, N.; Jacobs, D. M.; van Duynhoven, J.; Cannet, C.; Fang, F.; Humpfer, E.; Schafer, H.; Spraul, M.; Engelsen, S. B.; Smilde, A. K. Toward Reliable Lipoprotein Particle Predictions from NMR Spectra of Human Blood: An Interlaboratory Ring Test. *Anal. Chem.* **2017**, *89* (15), 8004−8012.
(17) Nicholson, J. K.; Foxall, P. J.; Spraul, M.; Farrant, R. D.; Lindon, J. C. 750 MHz ^{1}H and ^{1}H-^{13}C NMR spectroscopy of human blood plasma. *Anal. Chem.* **1995**, *67* (5), 793−811.
(18) Kimhofer, T. Metabom8. github.com/tkimhofer/metabom8.
(19) Dieterle, F.; Ross, A.; Schlotterbeck, G.; Senn, H. Probabilistic quotient normalization as robust method to account for dilution of complex biological mixtures. Application in ^{1}H NMR metabonomics. *Anal. Chem.* **2006**, *78* (13), 4281−90.

https://dx.doi.org/10.1021/acs.jproteome.0c00815
J. Proteome Res. 2021, 20, 1415−1423